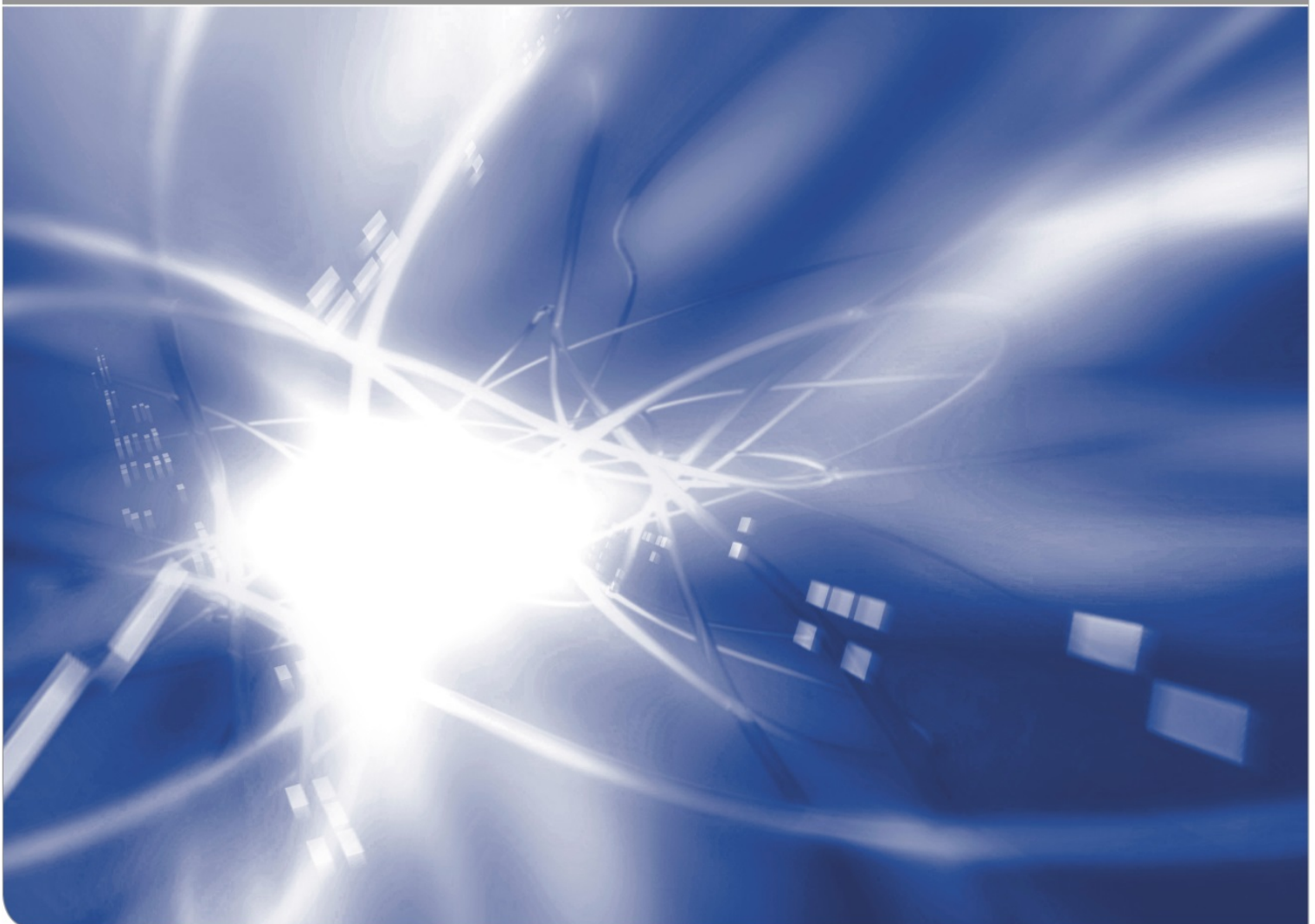


## **A contribution to stress-dependent vibration peaks**

- Asymmetric stretching mode
- Uniaxial loading

K. Günter Schell, Claudia Bucharsky, Susanne Wagner, Theo Fett

KIT SCIENTIFIC WORKING PAPERS **250**



# Institute for Applied Materials

## Impressum

Karlsruher Institut für Technologie (KIT)  
www.kit.edu



This document is licensed under the Creative Commons Attribution – Share Alike 4.0 International License (CC BY-SA 4.0): <https://creativecommons.org/licenses/by-sa/4.0/deed.en>

2024

ISSN: 2194-1629

## **Abstract**

An interesting effect in silica glass is the shift of IR- and Raman-peaks under externally applied stresses. A first interpretation of the influence of stress on the IR frequency was made possible by its influence on the bond angles, as had been shown very early by Galeener [1]. In this interpretation, the stress effect is assumed as a consequence of a change of the bond angles due to the stresses.

In the following section we will show that the angle stretching is not the only effect that influences the position of the frequency of IR lines. The present Report will address the change in the peak position under uniaxial tension and compression in the so-called asymmetric stretching mode (AS). For our computations we used Lennard-Jones potential.

From our computations, we have to expect decreased frequency under tension and increased frequency under compression loading. This result is in agreement with measurement by Tallant et al. [2].



# Contents

<b>1 Position of Raman-maximum in the absence of stresses</b>	<b>1</b>
1.1 Structure element and binding situation for silica	2
1.2 Description of a bond by the Lennard-Jones potential	2
<b>2 Effect of stresses</b>	<b>6</b>
<b>References</b>	<b>10</b>



## 1. Position of IR- and Raman-maxima in the absence of stresses

The interpretation of stress influences on the position of IR- and Raman-lines that has been dominant to date is based on Galeener's [1] suggestion. In our opinion, other effects are also possible that can also influence the position of the lines in the IR spectrum or the Raman spectrum. This report will address the change in the rest position of the oscillating system due to uniaxial external loads. An example for the influence of stresses are measurements by Tallant et al. [2], shown in Fig. 1 (“Frequency” in terms of the wavenumber).

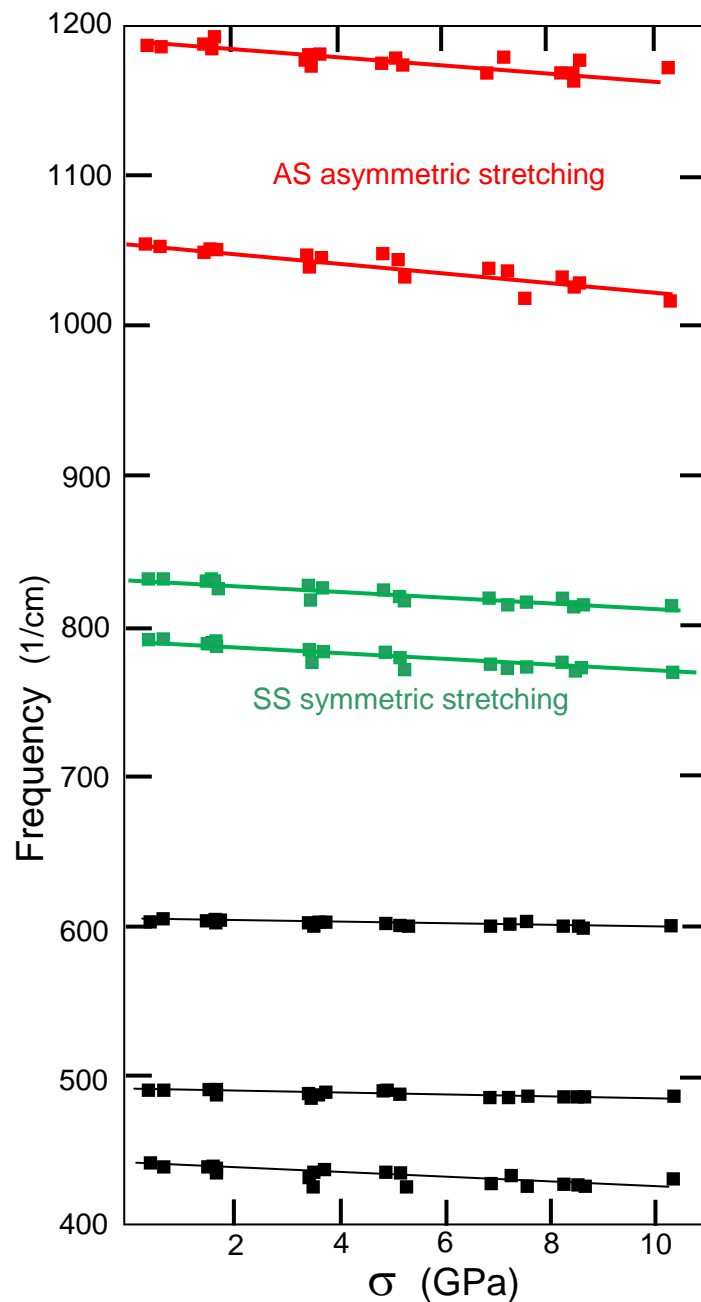


**Fig. 1** Measurements by Tallant et al [2] on silica by tensile tests.

## 1.1 Structure element and binding situation for silica

The infrared spectrum for silica glass shows a shifting of infrared peaks under stresses. The strongness and direction of the peak shift depends on the chosen IR-peak frequency and the surface state (water-affected, annealed, etched [3]). A first interpretation of the influence of stress on the IR frequency was made possible by its influence on the bond angles, as had been shown very early by Galeener [1]. Figure 2 shows a silica structural unit. The direction  $S$  represents the direction in which antisymmetric stretching (ASS) takes place,  $B$  stands for the so-called bending mode.

Galleener suggested for the dependency between the angular frequency  $\omega$  and the bond angle  $\theta$  for the special case of the antisymmetric stretching mode [1, 4]

$$\begin{aligned}\omega_1^2 &= (\alpha / m_O)(1 + \cos \theta) \\ \omega_2^2 &= (\alpha / m_O)(1 - \cos \theta)\end{aligned}\quad (1)$$

where  $m_O$  is the mass of the oxygen atom and  $\alpha$  a bond-stretching parameter. The parameters  $\alpha$  as well as  $\theta$  can depend on the global stress state, i.e.  $\alpha = \alpha(\sigma)$  and  $\theta = \theta(\sigma)$ . In the following section we will show that the angle stretching is not the only effect that influences the position of the frequency of IR lines.

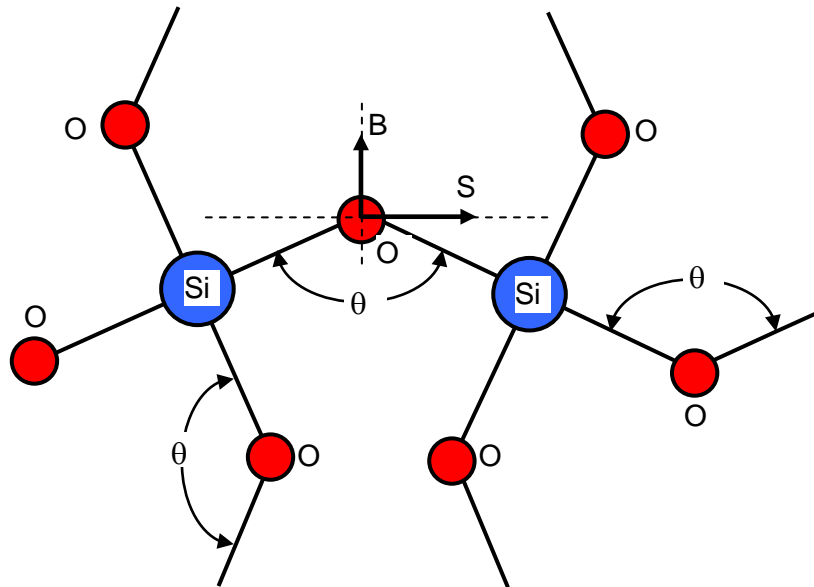


**Fig. 2** Schematic illustration of a silica structural unit with the Si-O-Si angles  $\theta$ . The arrow  $S$  stands for the stretching mode and  $B$  for the bending mode.

## 1.2 Description of a bond by the Lennard-Jones potential

In order to minimize the number of disturbing influences, we will consider bond-stretching first in the stress-free state, keeping  $\alpha$  and  $\theta$  as constants. For the interaction between Si and O atoms let us use a Lennard-Jones potential as given by eq.(2)

$$U = 4\epsilon_0 \left( \left( \frac{a}{r} \right)^{12} - \left( \frac{a}{r} \right)^6 \right) \quad (2)$$

In this relation  $a$  is a measure of the distance between the different atoms and  $\epsilon_0$  is the deepest point of the potential curve. The equilibrium distance  $r_0$  at which the first derivative of the potential disappears, is

$$\frac{dU}{dr} = 0 \Rightarrow r = r_0 = 2^{1/6} a \cong 1.12246 a \quad (3)$$

Figure 3 shows the Lennard-Jones potential, eq.(2), in normalized representation.

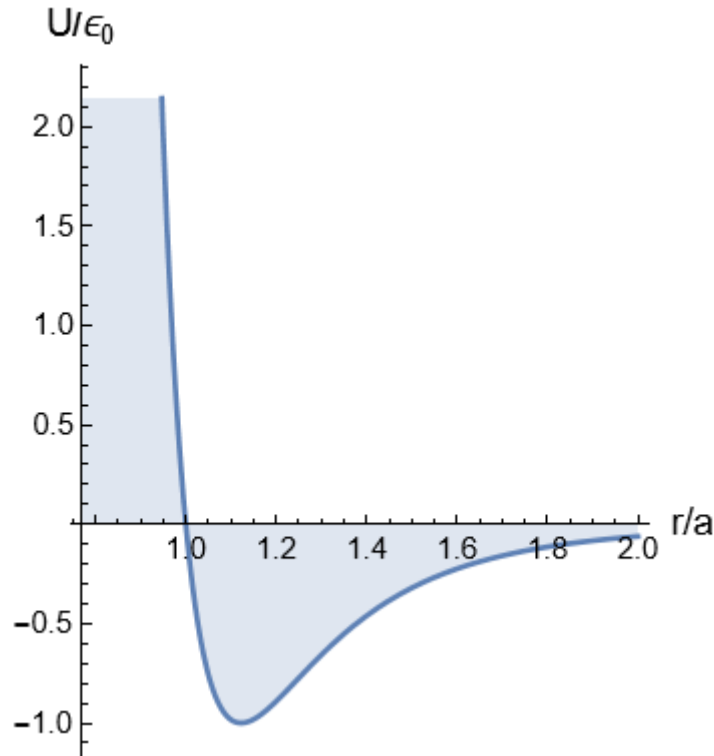


**Fig. 3** Lennard-Jones potential according to eq.(2) in normalized representation.

The force  $F$  that must be applied to increase the distance  $r$  between the two bonding partners is then given by

$$F = \frac{dU}{dr} = \frac{4\epsilon_0}{a} \left( -12 \left( \frac{a}{r} \right)^{13} + 6 \left( \frac{a}{r} \right)^7 \right) \quad (4)$$

This force is plotted as the red curve in Fig. 4.

The curvature of the potential curve provides the Hook parameter (or “spring constant”)  $k$ , the restoring force  $dF$  per extension  $dr$

$$k = \frac{dF}{dr} = \frac{d^2U}{dr^2} = \frac{4\epsilon_0}{a^2} \left( 156 \left( \frac{a}{r} \right)^{14} - 42 \left( \frac{a}{r} \right)^8 \right) \quad (5)$$

Figure 5 shows this dependency. The restoring force for  $r=r_0$ ,  $k_0$ , reflects the relationship between the force and the deflection from the equilibrium position. In our opinion there must exist an effect of externally applied stresses.

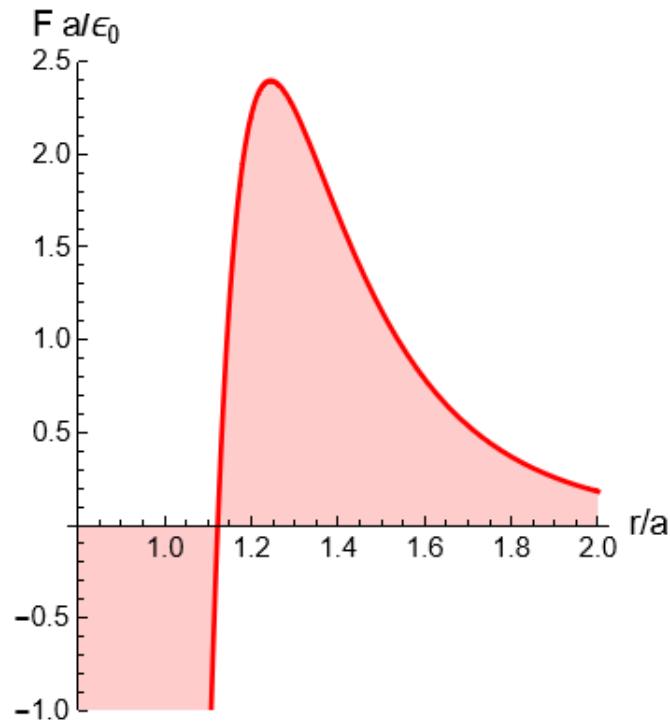


**Fig. 4** Restoring force  $F$  for the Lennard-Jones potential.

The dashed part in Fig. 5 with  $k < 0$  is without relevance for the computation of vibrations. The black circle represents the value at equilibrium,  $k=k_0$ , in the absence of external stresses on the bond. This point is given by

$$k_0 = \frac{4\epsilon_0}{a^2} \left( 156 \left( \frac{a}{r_0} \right)^{14} - 42 \left( \frac{a}{r_0} \right)^8 \right) = 36 \times 2^{2/3} \frac{\epsilon_0}{a^2} \cong 57.146 \frac{\epsilon_0}{a^2} \quad (6)$$

and introduced in Fig. 5 at  $r_0$ . The slope of the curve tangent at equilibrium results to be

$$\left. \frac{dk}{dr} \right|_{r_0} = \frac{4\varepsilon_0}{a^3} \left( -2184 \left( \frac{a}{r_0} \right)^{15} + 336 \left( \frac{a}{r_0} \right)^9 \right) = -756\sqrt{2} \frac{\varepsilon_0}{a^3} \quad (7)$$

By Taylor expansion of eq.(6) we obtain the linear approximation

$$k \cong k_0 - 756\sqrt{2} \frac{\varepsilon_0}{a^2} \left( \frac{r}{a} - 2^{1/6} \right) \quad (8)$$

which is introduced in Fig. 5 as the red straight line. The Taylor expansion for the force  $F$  is

$$F \cong k_0 a \left( \frac{r}{a} - 2^{1/6} \right) \quad (9)$$

and by combining eqs.(8) and (9) we obtain for the relation  $k=f(F)$  the linear approximation

$$k \cong k_0 - 21 \frac{F}{r_0} \quad (10)$$

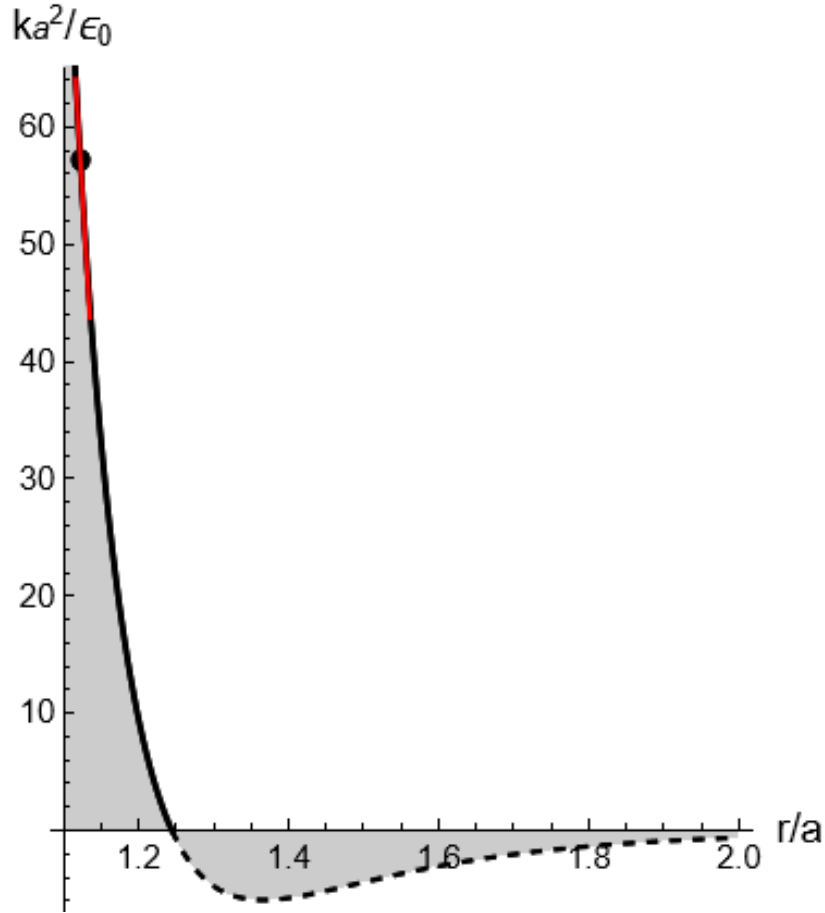


**Fig. 5** Curvature of the potential curve  $k \propto (d^2U/dr^2)$  as a function of  $r/a$ . Circle: Restoring force at equilibrium, red line: Taylor series approximation by eq.(8).

Finally, the mechanical properties resulting from the Lennard-Jones potential are compiled once more in Fig. 6. The restoring force is plotted here as  $1/10 \times k a^2/\epsilon_0$ , in order to apply the same ordinate scaling for all the curves.

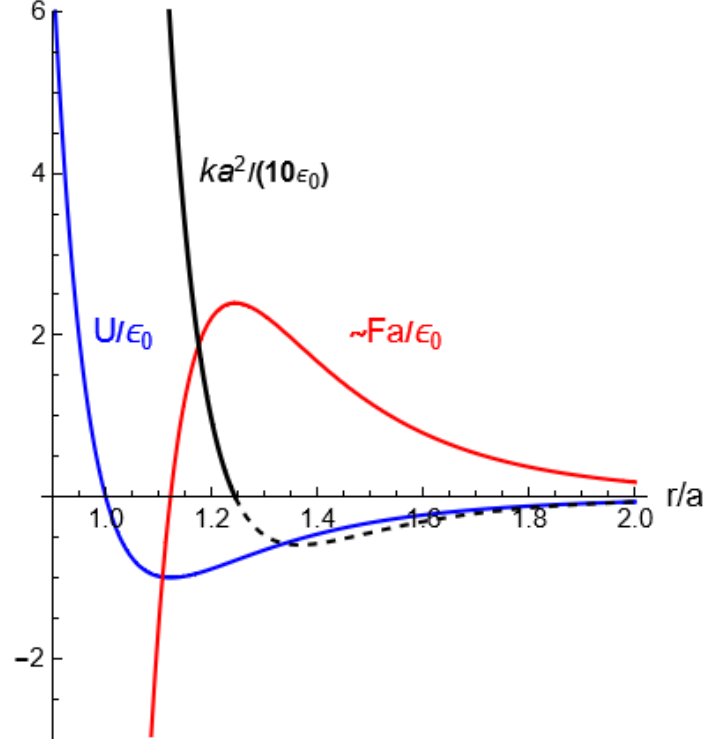


**Fig. 6** Mechanical properties derived from the Lennard-Jones potential, blue: Potential  $U/\epsilon_0$ , red: binding force  $Fa/\epsilon_0$ , black: restoring force  $1/10 \times k a^2/\epsilon_0$ , in order to use the same ordinate scaling for all the three curves.

## 2. Effect of stresses

An axially applied stress  $\sigma_{\text{appl}}$  leads to a tensile force  $F_{\text{appl}}$  in the  $r$ -direction, which can be roughly estimated by

$$F_{\text{appl}} \approx a^2 \sigma_{\text{appl}} \quad (11)$$

When this external load  $F_{\text{appl}}$  is applied, a new equilibrium position results at the intersection of the binding force  $F(r)$  with the externally caused force  $F_{\text{appl}}$  (see Fig. 7). The new balance is symbolized by the red circle. Under compressive stresses, we obtain the green line with the green circle indicating the intersection with the binding force curve.

Whereas for the stress-free case the eq.(6) holds with  $k=k_0=57.14 \epsilon_0/a^2$ , we obtain for tension loading  $F_{\text{appl}}=+1/2 \epsilon_0/a$  with  $k=47.65 \epsilon_0/a^2$  and for compressive load  $F_{\text{appl}}=-1/2 \epsilon_0/a$  the result of  $k=66.39 \epsilon_0/a^2$ . The “spring constant”  $k$  and the vibration frequency  $\nu$  are related by

$$v = \sqrt{\frac{k}{m}} \quad (12)$$

where  $m$  is the “reduced molecule mass”. All results obtained from the Lennard-Jones potential are compiled in Table 1.

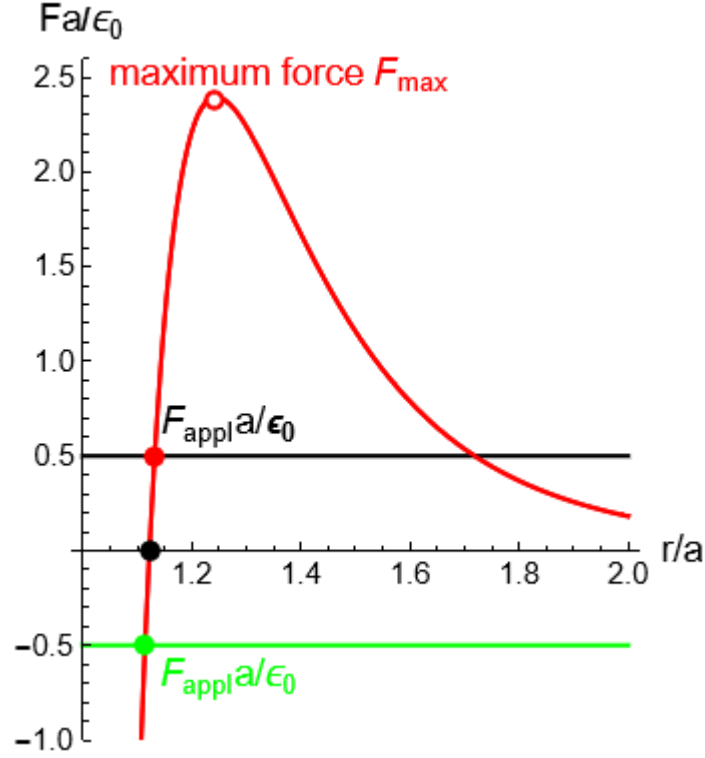


**Fig. 7** Binding forces under externally applied forces  $F_{\text{appl}}$ .

loading $F_{\text{appl}} \times a / \epsilon_0$	$r/a$	$k a^2 / \epsilon_0$	$k/k_0$	$v/v_0$
+1/2	1.1320	47.654	0.8339	0.913
0	1.1224	57.145	1	1
-1/2	1.1143	66.391	1.1618	1.078

**Table 1:** Results from computations on the Lennard-Jones potential.

Figure 8 finally indicates the shift of  $k$  by the external stresses (see also eq.(10)). The most important result of our study is the fact, that externally applied uniaxial loading must change the frequency of molecular vibrations. We have to expect a decreased frequency under tension and an increased frequency under compression loading.

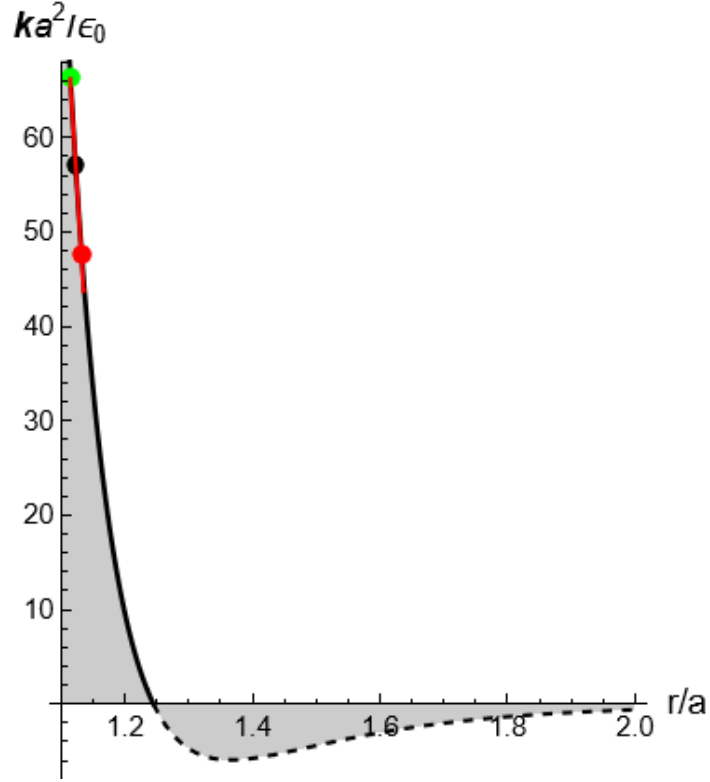


**Fig. 8** Binding forces under externally applied forces  $F_{\text{appl}}$ . Circles: Black without stress, red under tension, green under compression.

The linear relation between spring constant  $k$  and externally applied force  $F=F_{\text{appl}}$ , eq.(10), is of course sufficiently correct for small forces compared with the maximum force  $F_{\text{max}}$ , with the value of

$$F_{\text{max}} = \frac{252}{169} \left( \frac{7}{13} \right)^{1/6} 2^{5/6} \frac{\epsilon_0}{a} \cong 2.396 \frac{\epsilon_0}{a} \quad (13)$$

and the location

$$r(F_{\text{max}}) = \left( \frac{26}{7} \right)^{1/6} a \quad (14)$$

In order to be able to assess the accuracy of the approximation eq.(10), the curve  $k(F)$  was calculated (black curve) and compared in Fig. 9 with the linear approximation (red line). From Fig. 9, we can conclude that the linear approximation is sufficient in the region of  $-2 < F < 1$  with maximum deviations of 1.7%.

Finally, Fig. 10 represents the dependency in a normalized form

$$\frac{k}{k_0} = f\left(\frac{F_{\text{appl}}}{F_{\text{max}}}\right) \quad (15)$$

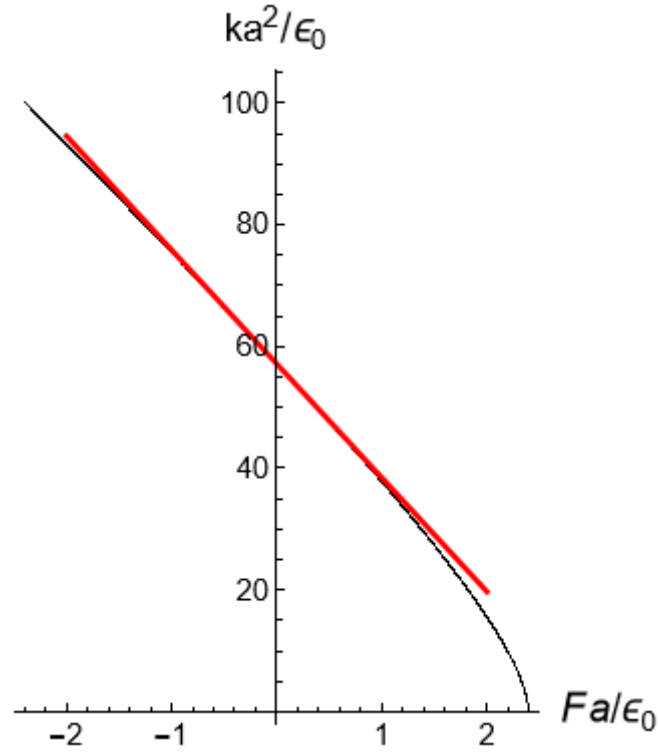


**Fig. 9** Dependency  $k=f(F)$ , given by the black curve, linear approximation eq.(10) by the red line.

Because of eq.(11) the relation (15) can be expressed also in terms of stresses

$$\frac{k}{k_0} = f\left(\frac{\sigma_{appl}}{\sigma_0}\right) \quad (16)$$

where  $\sigma_0$  is the so-called ideal strength and  $\sigma_{appl}$  stands for the applied stress. The ideal strength is of course larger than all measured strengths and could only occur if no surface cracks are present in test fibers. From measurements by Brambilla and Payne [5] on extremely thin silica fibers of about 60 nm radius, one can conclude that  $\sigma_0$  may exceed 25 GPa.

We therefore suggest using the following linear approximation up to an applied stress of around  $\sigma_{appl}/\sigma_0=0.4$ :

$$\frac{k}{k_0} \cong 1 - \frac{147}{169} \left(\frac{7}{13}\right)^{1/6} \frac{\sigma_{appl}}{\sigma_0} \quad (10a)$$

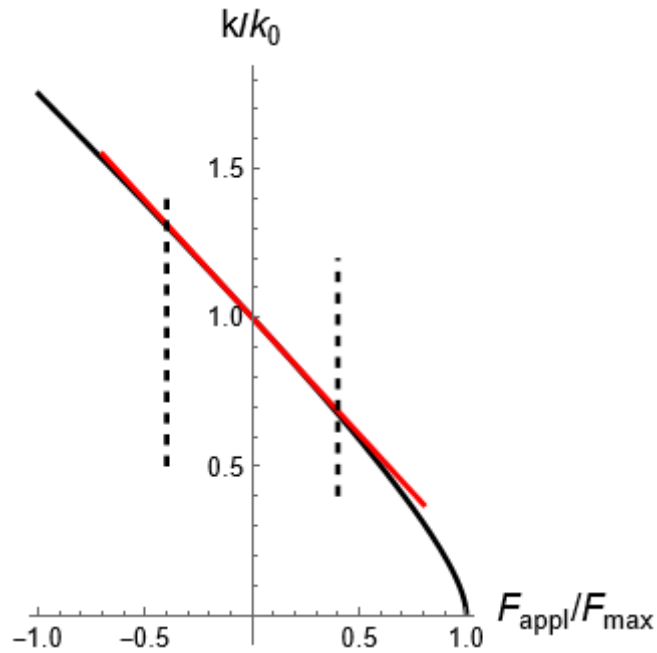


**Fig.10** Normalized representation of Fig. 9 with the applied load  $F_{\text{appl}}$  scaled on the maximum possible force  $F_{\text{max}}$ . Dashed lines: limits for the suggested linear solution, eqs.(10, 10a).

**Conclusion:** By application of the Lennard-Jones potential, it can be shown that the effect of stresses on the peak positions of Raman- and IR-spectra in silica is a shift to lower frequency under tensile loading and to higher frequency under compression loading. This result is in good agreement with the measurements by Tallant et al. [2]. In a following study, we will address also multiaxial stress states as for instance equibiaxial and hydrostatic compression.

## References

- 1 F.L. Galeener, Band limits and the vibrational spectra of tetrahedral glasses, *Phys. Rev. B*, **19** (1979), 4292-4297.
- 2 Tallant DR, Michalske TA, Smith WL. 1988. *J. Non-Cryst Solids* 106: 380-82
- 3 M. Tomozawa, Y.-K. Lee, Y.-L. Peng, Effect of uniaxial stresses on silica glass structure investigated by IR spectroscopy, *Journal of Non-Crystalline Solids* **242** (1998), 104-109.
- 4 P.N. Sen and M.F. Thorpe, *Phys. Rev. B* **15** (1977), 4030 pp.
- 5 G. Brambilla, D.N. Payne, The ultimate strength of glass silica nanowires, *Nano Letters*, **9**(2009), 831-835.



KIT Scientific Working Papers  
ISSN 2194-1629

[www.kit.edu](http://www.kit.edu)